



CdS-deposited titania nanotubes array heterostructures and its investigation for photocatalytic application under visible light

R DELMA JONES RUFINA and PERARASU THANGAVELU* 

Thermal and Bio Analysis Laboratory, Department of Chemical Engineering, Anna University, Chennai 600 025, India

*Author for correspondence (vtparasu@annauniv.edu)

MS received 13 February 2022; accepted 5 May 2022

Abstract. Titania is a fantastic photocatalyst, although visible excitation is the gold standard due to its broader bandgap. As a solution, doping is used to boost visible light excitation. Cadmium sulphide (CdS) is another well-known photo-material that forms the best photocatalyst when combined with titania. Because of its organized architecture and large surface area compared to nanoparticles, the nanotubes array draws our attention among the many dimensions of nanomaterials. The conventional procedure for synthesizing titania nanotubes array by sonoelectrochemical synthesis was used in this study, and CdS doping was accomplished using a wet chemical process. Scanning electron microscope, X-ray diffraction and Fourier transform infrared were used to conduct morphological and compositional analyses. The optical studies were carried out at the same time using UV-visible, photoluminescence and UV-diffused reflectance spectroscopy characterization. CdS adhesion to titania is confirmed by bandgap shifting. To assist photocatalytic investigations, electrochemical impedance studies were conducted. Using a lab-prepared reactor, photocatalytic investigations were carried out, and a plausible mechanism was presented. CdS on TiNTs has a unique flower-like morphology, which has been reported elsewhere, and it demonstrates excellent adhesion, forming the best photocatalytic pair.

Keywords. Anodization; CdS; titania nanotubes array; nano photocatalyst; thin film coating; CdS doped; heterostructures; bandgap shifting.

1. Introduction

Nanomaterials have emerged as the research hero of this decade [1]. It is exciting to manipulate and analyse materials at the nanoscale. Nano photocatalyst is not an outlaw when it comes to performing miracles in fields like bioremediation [2], dermatology [3] and photoelectrochemical [4] applications. Nano is not just a word; it is also the foundation for a lot of studies. Nanomaterials have been with us, although invisibly, since the dawn of time. Richard Feynman's 'There's Plenty of Room at the Bottom' speech catapulted it into the spotlight [5]. The researchers began searching the rooms at the bottom after that. Those rooms are full of treasures and are continuously being explored. Nanomaterials are distinguished from bulk materials by their extraordinary physical and chemical characteristics. Nanomaterials come in a variety of sizes, including 1D nanoparticles, 2D nanowires [6] and 3D hollow structures [7] (e.g., nanotubes, fullerenes, etc.).

Nanomaterial manipulation is really exciting, and the applications are mind-boggling. Nanomaterials have a variety of important applications, including solar hydrogen [8], fuel cells [9], batteries [10], sensors [11], the aeronautics industry [12], thermoelectric devices [13] and

pharmaceuticals [14,15]. Titania is a well-known photocatalyst that has been used in a variety of applications over the last decade, including the degradation of organic contaminants [16,17], as a UV-resistant material [18], self-cleaning ceramics and glass [19], and the manufacture of cosmetic products [20] such as sunscreen creams and skin milk. Fujishima and Honda [21] pioneered research on the photolysis of water using titania as an anode in 1972, sparking interest in its photoelectrochemical applications [22,23].

Titania is being investigated in all nanoscale dimensions and, due to its larger surface area, it exhibits superior photocatalytic performance as a nanophotocatalyst. Titania nanotubes array (TiNTs) is an organized architecture of nanotubes generated by anodization on a titanium plate. While the high surface-to-volume ratio is the most distinguishing feature [24,25], the ordered design of TiNTs also provides a comparable and equivalent electric channel for electron transport [26] in the photoelectrochemical cell. Titania has a broad bandgap energy of around 3.2 eV, which can be boosted only in the UV region [27], necessitating doping to obtain visible light stimulation. Cadmium sulphide (CdS) is a semiconductor that is frequently used to couple with titania due to its narrow bandgap energy of

2.4 eV [28–30]. This combination is extremely important in the realm of photocatalysis because it enables excitation and electron hopping in the visible light spectrum.

The methodology for synthesizing TiNTs in this study was sonoelectrochemical anodization. Sonoelectrochemical anodization accelerates the synthesis of TiNTs on titanium plates in the presence of 10% ammonium fluoride in ethylene glycol electrolyte. CdS nanoparticles were made separately using the chemical reduction technique. In the chemical reduction technique, reducing agents such as ammonia or ammonium sulphide were used to reduce cadmium and sulphur precursors. The dip-coating method was used to apply the thin-film coating (i.e., just placing an anodized plate on top of the CdS nanoparticle dispersion). Morphological and compositional analyses were carried out using scanning electron microscope (SEM), X-ray diffraction (XRD) and Fourier transform infrared. UV–visible, photoluminescence and UV–diffused reflectance spectroscopy (DRS) characterization were used in the optical investigations.

TiNTs have an organized structure that favours superior photocatalytic use when compared to unbound nanotubes. CdS thin film-coated TiNTs are shown to have heterostructures by the compositional analysis and morphological analyses, respectively. Flower-like morphological structure, which was formed by applying a thin layer of coating is very unique and not reported elsewhere. Tauc plot was used to figure out the bandgap in this case. Detection of bandgap shifts confirms CdS adherence to titanium. A technique known as bandgap shifting could help boost the amount of visible light emitted by the photocatalyst. There is a strong handshake between the experiment results, proving visible light excitation successful. Using methyl orange (MO) dye degradation in a compact self-prepared reactor, TiNTs and CdS–TiNTs were examined for photocatalytic activity. Using photodegradation as a method of testing, an explanation for how it works was posited.

To better understand electron–hole pair generation and charge transit, the mechanism is suggested. The sandwich model, which consists of a UV-excited semiconductor (TiNT) and a visible light-excited semiconductor (CdS thin film coating), may effectively improve solar energy consumption in the visible light area. Photons impinge on CdS thin film coatings, which have a narrow energy bandgap compared to TiNT's broader bandgap, forming electron–hole pairs. The conduction band and valence band of TiNT are lower than those of CdS. The band structure favours photogenerated electrons transfer from CdS to TiNTs and photogenerated holes transfer from TiNTs to CdS. Because TiNT is active in UV and CdS is active in visible light, simulated solar irradiation could excite both the CdS thin film and TiNTs. Only the CdS particles were activated when exposed to visible light. Photogenerated electrons are transmitted from the CdS thin film to the TiNTs. The proposed process is represented in detail in figure 1.

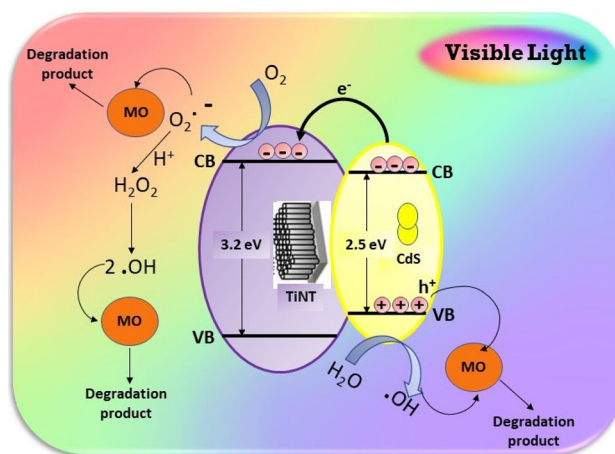


Figure 1. Schematic representation of degradation mechanism of methyl orange by CdS thin film-coated TiNTs.

2. Experimental

2.1 Materials and reagents

Aldrich Chemical Company supplied titanium sheets with a purity of 99.6% and a thickness of 1.0 mm. All other chemicals and solvents were acquired from Sigma Aldrich, and they were used exactly as they were purchased, with no further purification.

2.2 Formation of titania nanotubes

To achieve an equal surface, the titanium sheet was first sliced and mechanically polished. This first step is quite important. An even surface yields an even array of nanotubes. After polishing, it was etched chemically in a mixture of HF (hydrogen fluoride) and HNO₃ (nitric acid) for 10 min in an ultrasonic bath of ethanol. It was then cleaned with acetone and distilled water before being air-dried at room temperature. The titanium anode and platinum cathode were sonoelectrochemically anodized for 2.30 h in the presence of 10% ammonium fluoride in an ethylene glycol electrolyte at 40 V [31–33]. Anodization is an electrolytic technique that forms a thin oxide film (TiO₂) on a metal (Ti) surface. Ultrasonic waves were employed to aid anodization in sonoelectrochemical anodization. Instead of bending structures, this promotes the production of straighter nanotubes. Figure 2a displays the procedure. The titanium plate was sintered in a tubular furnace at 500°C in a nitrogen environment. Because the prepared sample was amorphous, this method was used to obtain crystalline TiNTs.

2.3 Thin-film coating

A magnetic stirrer was used to mix equal amounts of 0.02 M cadmium chloride and 1.5 M ammonium nitrate (let it be 20 ml each). To keep the pH at 8–9, drops of 0.8 M

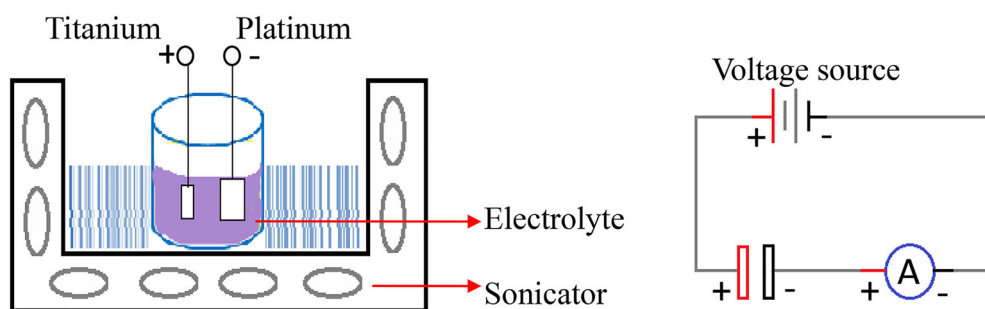


Figure 2. (a) Diagrammatic representation of sonoelectrochemical anodization. (b) Circuit diagram of the process.

potassium hydroxide were applied [34,35]. When the desired pH was reached, an equivalent amount of 0.2 M thiourea (20 ml) was added. The temperature should be kept at about 80°C. After a while, the colour changed to yellow, indicating the creation of CdS nanoparticles. CdS can be deposited as a thin film layer on the surface of TiNTs using the chemical bath deposition process, which involves immersing anodized titanium plates in a CdS bath. After that, the sample was dried in a hot air oven. The procedure was also attempted with the precursor cadmium sulphate to achieve distinct morphology.

3. Results and discussions

The XRD method was used to investigate the composition of the samples. XRD patterns were obtained using a Cu K radiation at 40 kV and 40 mA on an X-ray powder diffractometer. Additionally, the phase was confirmed using infrared (IR) spectroscopy. The powder obtained from the deposited films was analysed using an infrared (IR) spectrometer with a resolution of 1 cm^{-1} in the spectral range of 450–2000 cm^{-1} . A Hitachi SU1510 was used to examine the surface morphology of the CdS films. *Field emission scanning electron microscope* was used to make cross-sectional observations, and energy-dispersive X-ray spectroscopy (EDAX) experiments were used to confirm the contents. UV-absorption Vis's spectrometer with an optical integrating sphere was used to capture absorption spectra at wavelengths ranging from 300 to 800 nm. For bandgap research, UV-DRS was used. In addition to the morphological and structural examination, a photoluminescence study was conducted to confirm the nanostructured CdS covering. The photocatalytic degradation studies were carried out in a simple open-air reactor that had been developed in the laboratory. For photocatalytic tests, MO dye was utilized.

3.1 UV-vis spectroscopy

Figure 3 shows the UV-vis optical absorbance spectra of a produced CdS sample with wavelengths spanning from 350 to 800 nm [36–38]. The material's significant absorbance at

wavelengths below 520 nm, which corresponds to the CdS energy gap, was confirmed by the spectra. It was almost 520 nm at its highest point. A simple equation of $1240/\lambda$ is used to calculate the bandgap [39–41]. The obtained distinctive peak is referred to as λ . It was 520 nm in our instance. The formula was used to determine that the material has an E_g of 2.38 eV, which matches to CdS (2.4 eV). The visible light stimulation of the prepared sample in all photocatalytic applications [42,43] is evidenced by the bandgap.

3.2 XRD analysis

To get the sample for powder XRD, the thin layer-coated anodized titania was either treated to a peel-off method or the sample was simply scratched mechanically. Figure 4 depicts the XRD patterns of the thin film-coated anodized titanium plate along with as-prepared CdS and anodized Ti. The as-prepared CdS exhibit peaks at $2\theta = 25^\circ, 26.5^\circ, 28.2^\circ, 43.8^\circ, 47.8^\circ$ and 51.9° , which correspond to (100), (002), (101), (110), (103) and (112) planes (JCPDS 41-1049) [44]. The main diffraction peaks of TiO_2 exhibit peaks at $2\theta = 25.45^\circ, 37.95^\circ, 48.20^\circ, 53.9^\circ, 55.16^\circ$ and 62.81° , which correspond to (101), (004), (200), (101),

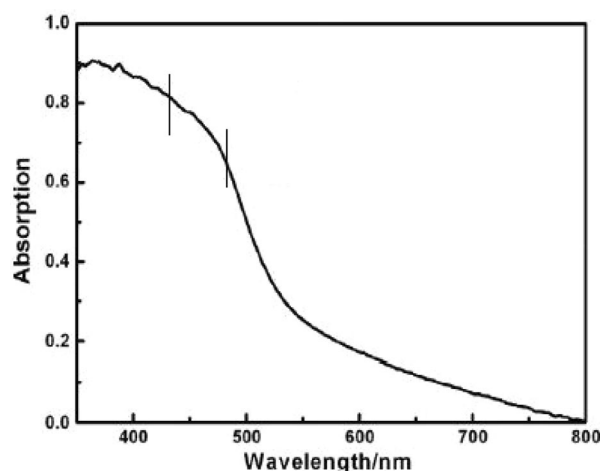


Figure 3. Optical absorption spectrum of CdS thin film-coated TiNTs.

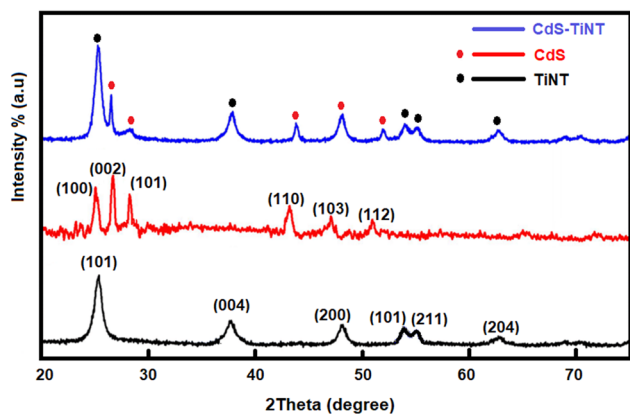


Figure 4. XRD patterns of CdS thin film-coated TiNTs.

(211) and (204) planes, respectively, with reference to JCPDS 21-1272 [45,46]. The hybrid structure exhibits the combination of both CdS and TiNT.

3.3 IR spectroscopy

Figure 5 shows the IR transmittance spectra of TiO_2 (TiNTs) and CdS– TiO_2 (CdS thin film-coated TiNTs) and the as-prepared CdS samples across the range of $450\text{--}2000\text{ cm}^{-1}$. The wide peak in the $400\text{--}600\text{ cm}^{-1}$ range for TiNTs is due to the active transverse optical (TO) vibration of the Ti–O bonds. It is associated to the longitudinal optical (LO) vibrational mode in the $700\text{--}950\text{ cm}^{-1}$ region. For the anatase phase, these features correspond to the TO and LO modes. The prominent signal at 1400 cm^{-1}

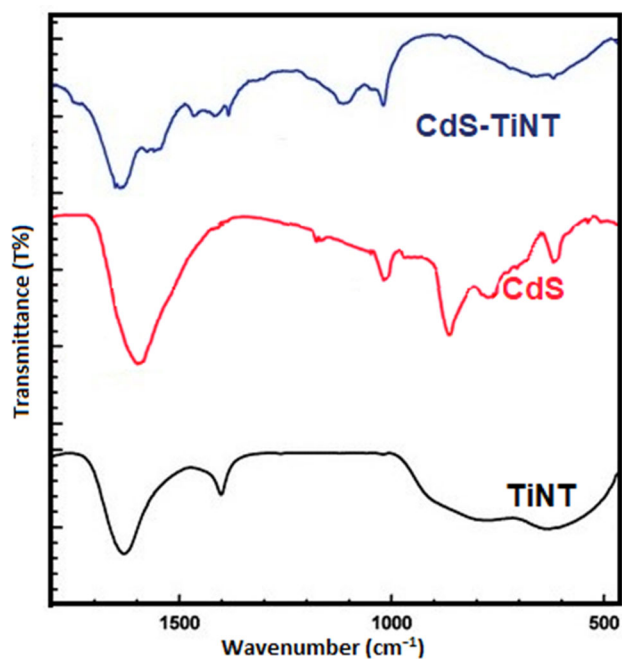


Figure 5. FT-IR spectra of TiNTs and CdS thin film-coated TiNTs.

indicates TiO_2 lattice vibrations. The absorption band at 1627 cm^{-1} was created by coordinated H_2O molecules bending vibrations and Ti–OH bonding. The vibration absorption peak in the CdS–TiNT sample is 619 cm^{-1} due to Cd–S stretching. In the CdS– TiO_2 sample, a broad peak centred at 664 cm^{-1} can easily be recognized. Peaks at 1040 , 1116 and 1645 cm^{-1} indicate the presence of CdS nanoparticles. The presence of both TiO_2 and CdS can be seen in the stretching and patterning, showing that CdS is coated thinly over TiNTs.

3.4 SEM characterization

The morphological investigations of nanomaterials need the use of a SEM. Figure 6 exhibits SEM micrographs of TiNTs and TiNTs covered with CdS thin film. We employed different cadmium precursors to achieve diverse morphologies, and it worked very well. Figure 6a and b shows the uniform TiNTs as prepared at two different magnifications. The pores are of the same size, and the tubes are evenly spaced. The SEM micrographs of CdS thin film-coated TiNTs generated using cadmium chloride precursor are shown in figure 6c, d and e. It shows the TiNTs with gorgeous shimmering flower-shaped coatings. The micrographs in figure 5g and h show CdS thin film-coated TiNTs produced with cadmium sulphate precursors. Over TiNTs, the sulphate precursor produces spherical-structured CdS coatings. The TiNTs and CdS-coated TiNTs were highlighted in the figures with red and yellow islands, respectively. Figure 5f depicts a sample of an unanodized titanium plate that has been coated. It did not appear to have any nanostructures on it. This demonstrates that TiNTs served as a template for CdS coating, resulting in flawless heterostructures.

The cross-sectional micrograph and EDAX spectrum are shown in figure 7. The length of the TiNTs seen in figure 7a was around 1 μm , but it was around 1.2 μm in figure 7b. CdS-coated TiNTs are exhibited in figure 7b, and the related EDAX spectrum is shown in figure 7d. The presence of Ti, O, Cd and S components are confirmed by the EDAX spectrum. Ti was more dominating than CdS in the micrograph because it was taken in cross-section. The bottom of TiNTs (i.e., the section that was attached to the titanium plate and oxide layer) is seen in figure 7c. This was achieved through the use of either a peeling technique (anodization with breaks) or a simple mechanical scratching process.

3.5 Bandgap studies using UV–DRS

Over the titanium plate, TiNTs were produced. UV–DRS was used to investigate bandgaps. The UV–DRS spectra of TiNTs and TiNTs coated with CdS are shown in figure 8a. Due to TiNTs' broad energy bandgap, its absorption is

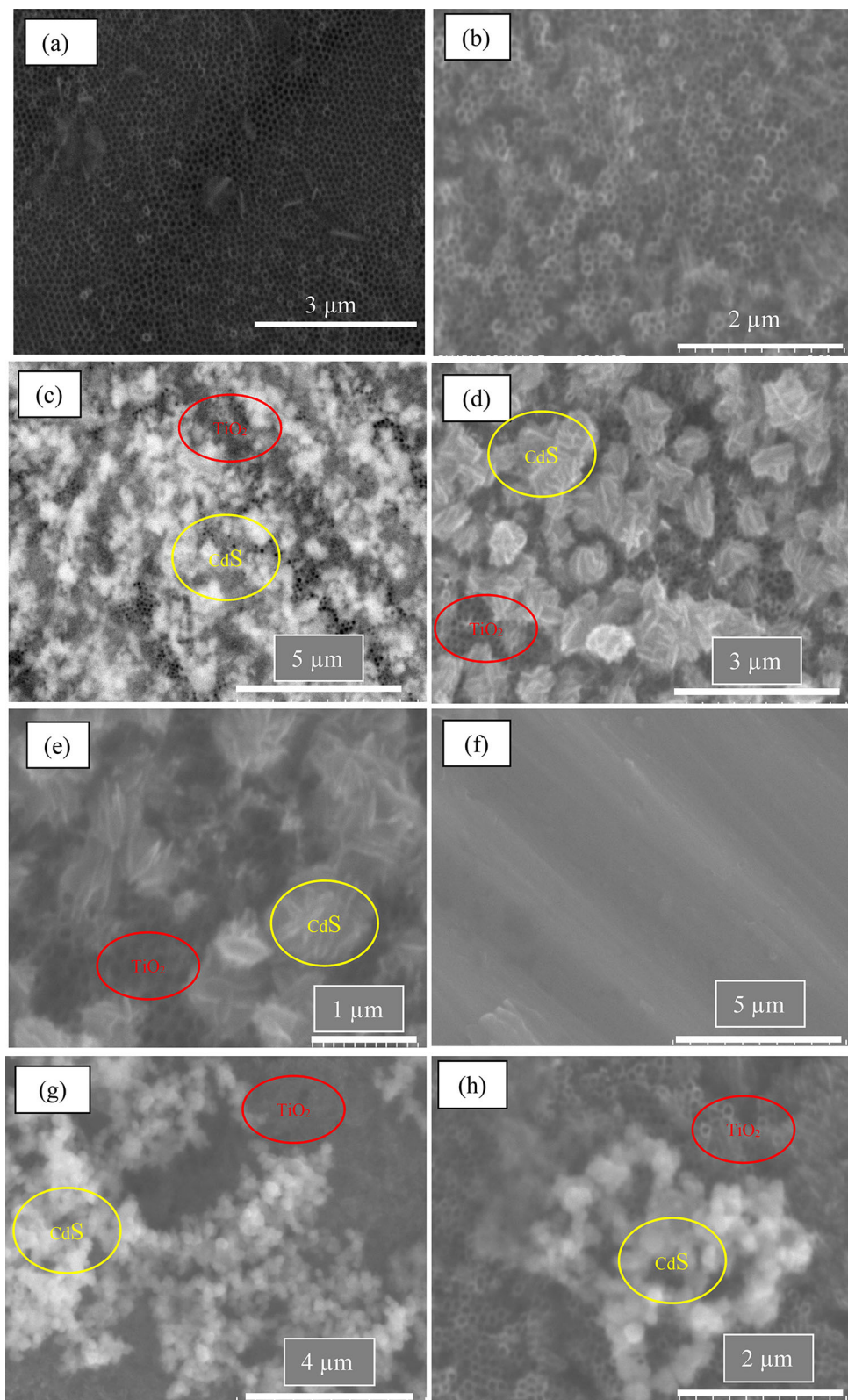


Figure 6. SEM micrographs of (a and b) TiNTs; (c, d and e) CdS thin film (from cadmium chloride precursor) coated TiNTs; (g and h) CdS thin film (from cadmium sulphate precursor) coated TiNTs; (f) CdS thin film coating attempted on titanium plate (without anodization).

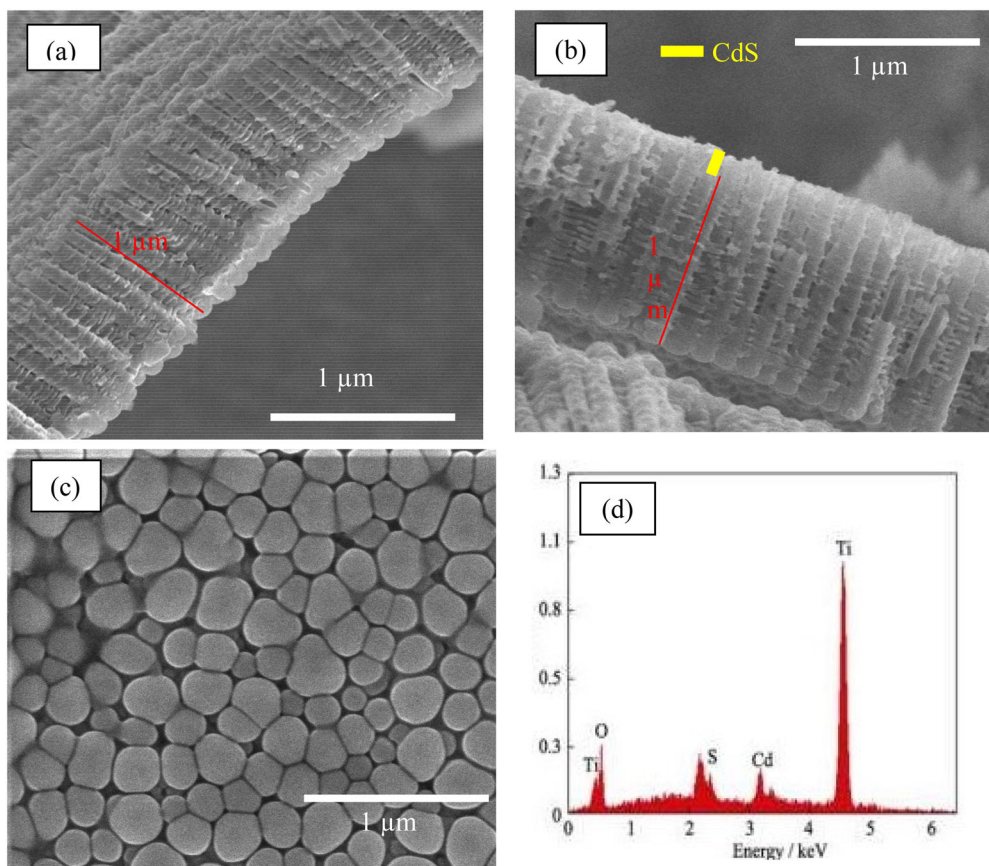


Figure 7. SEM micrograph of (a) cross-section TiNTs; (b) cross-section of CdS thin film-coated TiNTs; (c) backside of TiNTs after getting peeled from the substrate and (d) EDAX spectrum of cross-section of CdS thin film-coated TiNTs.

primarily in the UV area. As a result, no appreciable absorbance was seen in the visible region (3.2 eV). Contrary to popular belief, CdS-coated TiNTs have an absorbance peak in the 400–500 nm wavelength region, indicating visible light stimulation. The bandgap was calculated by plotting a tauc plot for CdS-coated TiNTs using the

Kubella–Munk function [47], as shown in figure 8b. The computed bandgap was 2.51 eV, confirming the CdS coating once more.

3.6 Photoluminescence studies

Photoluminescence spectroscopy (PL spectroscopy) is an excellent instrument for studying nanocrystalline thin films and nanomaterials. Figure 9 shows the PL spectrum for the sample in which CdS was coated onto TiNTs, which was recorded at a wavelength of 325 nm. The sample shows a large peak centred about 510 nm in the visible region. This range corresponds to the visible light spectrum’s green wavelength region, and hence to CdS’s green emission characteristics [48]. This validates the CdS thin film coating applied to TiNTs. In addition, the film’s transition peak is quite close to the bandgap calculated in the tauc plot. Also, PL spectra can be used to verify the efficiency of charge trapping and recombination of photo-induced electrons and holes in the semiconductor. CdS–TiNT exhibits weaker peak than TiNT. This shows that photo-induced electrons and holes have reduced recombinations.

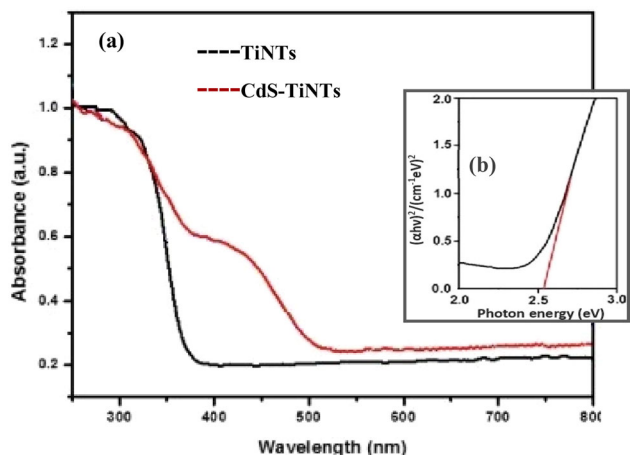


Figure 8. (a) UV–DRS spectrum of TiNTs and CdS–TiNTs. (b) Tauc plot for CdS–TiNTs spectrum.

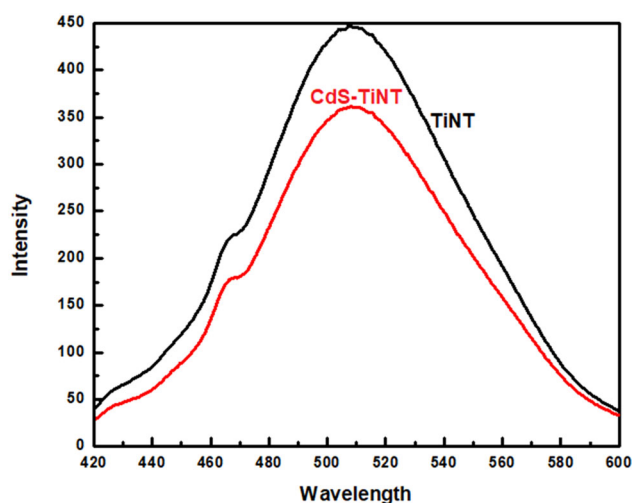


Figure 9. PL spectrum of CdS-coated TiNTs.

3.7 Photocatalytic studies

Under xenon lamp irradiation, the photocatalytic activity of TiNTs and CdS–TiNTs was evaluated by measuring the degradation of MO dye. In a lab-prepared closed-air reactor (as shown in figure 10), photocatalytic degradation tests for MO were performed. A 420 nm cutoff filter was used to obtain the visible light source. The materials were swirled in a beaker containing MO aqueous solution (25 mg l^{-1}) during the degrading process. The solution was agitated in the dark for 30 min before being irradiated with a 350-W xenon lamp to achieve dye adsorption equilibrium on the catalyst surface. Pipetting out of the reactor at regular intervals was used to describe the material. The solution's absorbance was measured using UV–vis absorption at a wavelength of 464 nm. The degradation of MO was assessed using a UV–Vis absorption spectrophotometer by observing the drop in concentration detected at the wavelength maximum (464 nm), as shown in figure 11a. The Beer–Lambert law was used to compute the MO degradation efficiency (D) [49].

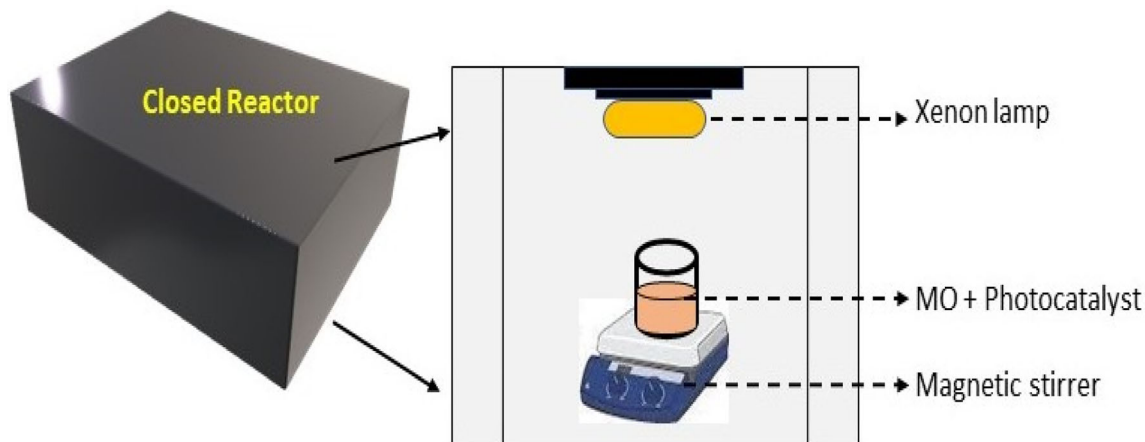


Figure 10. Lab-made closed air reactor for photocatalytic studies.

$$D = \frac{A_0 - A_t}{A_0} \times 100\%$$

The absorbance of the characteristic absorption peak of MO at 465 nm in aqueous solution before and after irradiation for a particular period is A_0 and A_t . The time-dependent photocatalytic degradation efficiency curves of TiNTs and CdS-coated TiNTs under simulated solar irradiation and visible irradiation, respectively, are shown in figure 11c and d. Under simulated solar irradiation, photodegradation efficiencies for TiNTs and CdS-coated TiNTs were 50.86 and 97.01%, respectively. The photocatalytic efficiency curves of TiNTs and CdS-coated TiNTs under visible light irradiation are shown in figure 11d. The efficiencies in this scenario are 2.63 and 42.25%, respectively. CdS-covered TiNTs displayed improved photocatalytic performance in both cases. The J – V characteristics of TiNT and CdS–TiNTs are shown in figure 11b. CdS-coated TiNTs exhibited an open-circuit voltage (V_{oc}) of 0.561 V and short-circuit current density (J_{sc}) of 6.85 mA cm^{-2} .

3.8 Cyclic voltammetry and electrochemical impedance studies

Cyclic voltammetry was employed to study the effect of the potential bias of CdS–TiNTs in dark and illumination. Photoelectrochemical behaviour of the catalysts was investigated in a standard three electrodes system, using saturated calomel as reference and platinum wire counter electrodes, respectively. The working electrode was CdS–TiNTs. Figure 12a shows a cyclic voltammogram recorded at the scan rate of 20 mV s^{-1} under illumination and dark. Figure 12b shows the electrochemical impedance spectra (Nyquist plots) generated for TiNTs and CdS–TiNTs. The charge carrier migration in an electrode system is identified using the Nyquist plot. The charge transfer resistance (R_{ct}) at the electrode interface is shown by the semicircle. Inset to figure 12b shows the analogous circuit fit used in this study.

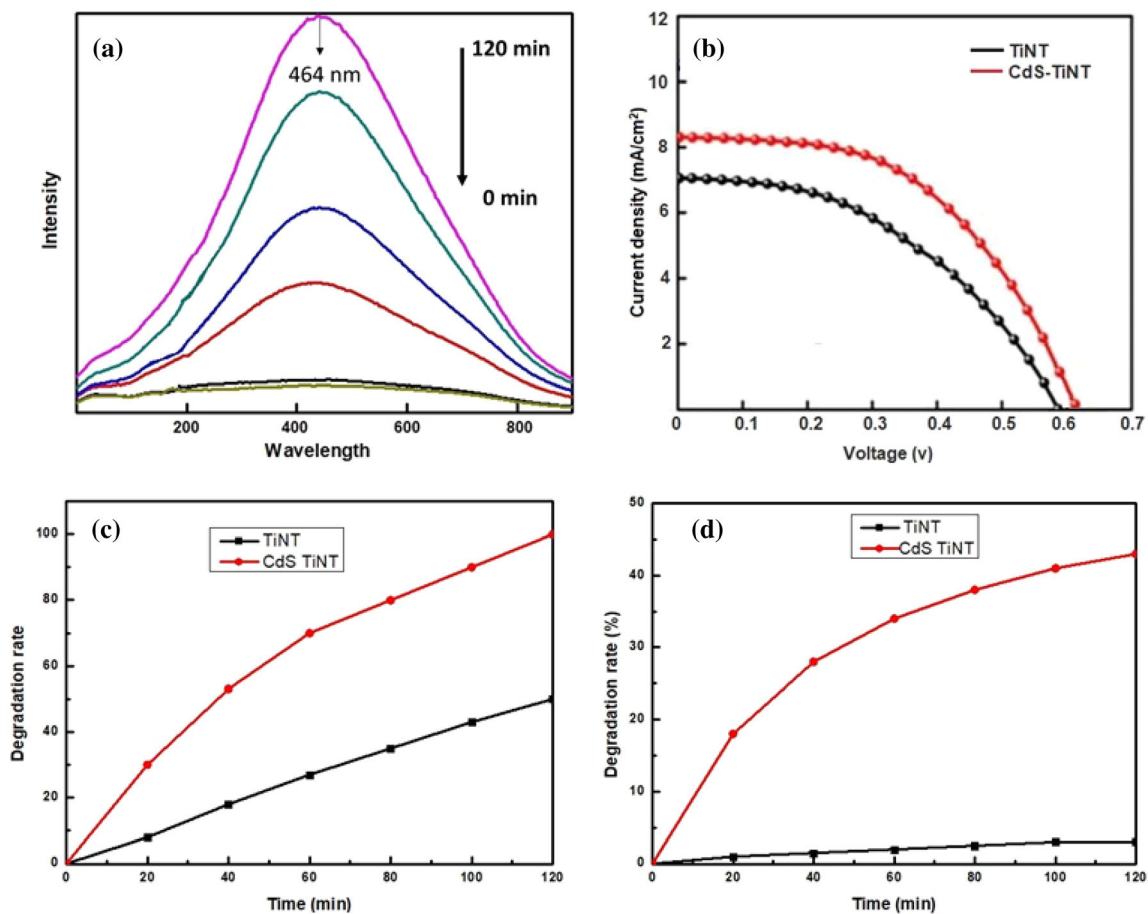


Figure 11. (a) Photocatalytic degradation of MO using CdS-TiNTs. (b) J - V characteristics. Degradation efficiency of methyl orange solution under (c) solar simulator radiation and (d) visible light irradiation.

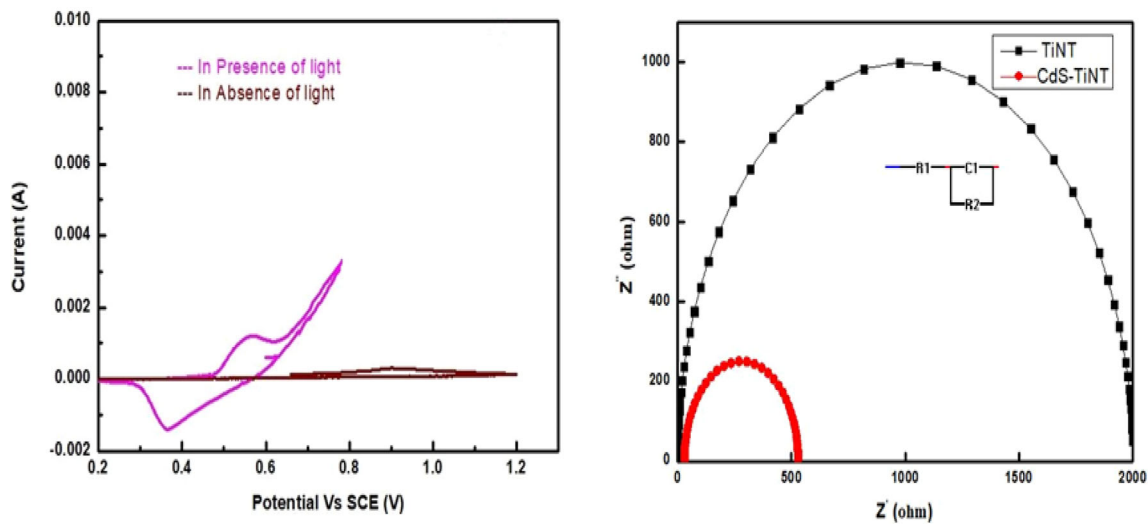


Figure 12. (a) Cyclic voltammogram of CdS-TiNTs under dark and illumination. (b) Electrochemical impedance spectra of TiNTs and CdS-TiNTs.

The x -intercept of the Nyquist plot determines R_1 , which describes the total resistance between the electrode and the electrolyte. The R_1 values for TiNTs and CdS–TiNTs were discovered to be 50.5 and 110.3, respectively.

The ability to store charge in the double layer of the semiconductor/electrolyte interface is referred to as space-charge capacitance (C_{SC}); the semicircle seen in the middle frequency region is referred to as interfacial charge transfer resistance (R_{ct}). The intra and inter-particle resistance, i.e., R_2 , has been claimed to be the main cause of charge transfer resistance. The shortest semicircle showed the fastest interfacial electron transport and effective separation of electron–hole pairs. This demonstrates the presence of CdS over TiNTs, which facilitated electron transport by promoting interfacial electron transfer between the electrode and the electrolyte interface. In CdS–TiNTs, CdS acted as an acceptor for TiO_2 's produced electrons, significantly lowering charge recombination and encouraging more charge carriers to form reactive species, enhancing dye degradation. As a result, charge carriers could be transported quickly, and effective charge separation could be obtained.

4. Conclusion

TiNTs were prepared by sonoelectrochemical anodization process, whereas CdS nanoparticles were synthesized through wet chemical method. TiNTs provide ordered architecture for all photocatalytic applications, comparative to that of other nanostructures. The heterostructures were obtained by the thin-film coating of CdS over TiNTs by the dip-coating method. Two different morphologies of thin-film coat were achieved by changing the cadmium precursor, which has not been reported elsewhere. The heterostructure combination of CdS and TiO_2 is demonstrated by compositional investigations. The stretching in Fourier transform infrared analysis indicates the bonding between the molecules, whereas XRD shows the combined peaks of TiO_2 and CdS. The materials' optical absorbance spectra and PL investigations also point to an optical bandgap for visible light excitation. The bandgap was computed using a tauc plot and found to be consistent with the PL results. Morphological investigations reveal ordered TiNTs in cross-section, as well as CdS-coated TiNT in appealing shapes. A potential substance, MO, was chosen to explore the light degradation mechanism, and a possible mechanism was provided. In general, TiO_2 was photocatalytically active only in the UV range. The optical investigations show that CdS adheres to TiNTs. As a result, the photocatalytic application in visible light is supported by titania nanostructures paired with CdS thin film. In addition, it was demonstrated that TiNTs and CdS heterostructures create the best visible light excitation pair in all photocatalytic applications.

References

- [1] Zeng L, Xiao L, Zhang J and Fu H 2020 *J. Nanosci. Nanotechnol.* **20** 4607
- [2] Joodi A, Allahyari S, Rahemi N, Hoseini S and Tasbihi M 2020 *Ceram. Int.* **46** 11328
- [3] Li Y, Yang D, Lu S, Qiu X, Qian Y and Li P 2019 *ACS Sustain. Chem. Eng.* **7** 6234
- [4] Li Z, Bian H, Xiao X, Shen J, Zhao C, Lu J *et al* 2019 *ACS Appl. Nano Mater.* **2** 7372
- [5] Feynman R 2018 *Feynman and computation* (CRC Press, UK) p 63
- [6] He Z, Zhang J, Li X, Guan S, Dai M and Wang S 2020 *Small* **16** 2005051
- [7] Yang J J, Li Z W, Liu X Y, Fang W H and Cui G 2020 *Phys. Chem. Chem. Phys.* **22** 19542
- [8] Tahir M B, Malik M F, Ahmed A, Nawaz T, Ijaz M, Min H S *et al* 2021 *Int. J. Environ. Anal. Chem.* **101** 2255
- [9] Duolikun T, Thomas P, Lai C W and Leo B F 2020 *Magnetochem. Mater. Appl.* **66** 217
- [10] Xu X, Xiong F, Meng J, Wang X, Niu C, An Q *et al* 2020 *Adv. Funct. Mater.* **30** 1904398
- [11] Malik R, Tomer V K, Mishra Y K and Lin L 2020 *Appl. Phys. Rev.* **7** 021301
- [12] Zotti A, Zuppolini S, Borriello A and Zarrelli M 2020 *Nanomaterials* **10** 1388
- [13] Kogo G, Xiao B, Danquah S, Lee H, Niyogushima J, Yarbrough K *et al* 2020 *Sci. Rep.* **10** 1
- [14] Deng Y, Zhang X, Shen H, He Q, Wu Z, Liao W *et al* 2020 *Front. Bioeng. Biotechnol.* **7** 489
- [15] Nasrollahzadeh M, Sajjadi M, Soufi G J, Irvani S and Varma R S 2020 *Nanomaterials* **10** 1072
- [16] Feng Y, Rijnaarts H H, Yntema D, Gong Z, Dionysiou D D, Cao Z *et al* 2020 *Water Res.* **186** 116327
- [17] Xu Y, Ahmed R, Klein D, Cap S, Freedy K, McDonnell S *et al* 2019 *J. Power Sour.* **414** 242
- [18] Wei W, Lü X, Jiang D, Yan Z, Chen M and Xie J 2014 *Dalton Trans.* **43** 9456
- [19] Mor G K, Varghese O K, Paulose M and Grimes C A 2003 *Sens. Lett.* **1** 42
- [20] Wakefield G, Green M, Lipscomb S and Flutter B 2004 *Mater. Sci. Technol.* **20** 985
- [21] Fujishima A and Honda K 1972 *Nature* **238** 37
- [22] Lu Y H, Xu B, Zhang A H, Yang M and Feng Y P 2011 *J. Phys. Chem.* **115** 18042
- [23] Regonini D and Clemens F J 2015 *Mater. Lett.* **142** 97
- [24] Shin Y and Lee S 2008 *Nano Lett.* **8** 3171
- [25] Montakhab E, Rashchi F and Sheibani S 2020 *Appl. Surf. Sci.* **534** 147581
- [26] Zhang Z, Wang Q, Xu H, Zhang W, Zhou Q, Zeng H *et al* 2020 *Electrochem. Commun.* **114** 106717
- [27] Liang H C, Li X Z and Nowotny J 2010 *In Solid State Phenom.* **162** 295
- [28] Kaur M, Mehta S K and Kansal S K 2018 *J. Environ. Chem. Eng.* **6** 3631
- [29] Deshpande A and Gupta N M 2010 *Int. J. Hydrog. Energy* **35** 3287
- [30] Ju L, Dai Y, Wei W, Li M, Liang Y and Huang B 2018 *Phys. Chem. Chem. Phys.* **20** 1904

- [31] Mor G K, Shankar K, Varghese O K and Grimes C A 2004 *J. Mater. Res.* **19** 2989
- [32] Cai Q, Paulose M, Varghese O K and Grimes C A 2005 *J. Mater. Res.* **20** 230
- [33] Varghese O K, Paulose M and Grimes C A 2009 *Nat. Nanotechnol.* **4** 592
- [34] Zhai T, Fang X, Li L, Bando Y and Golberg D 2010 *Nanoscale* **2** 168
- [35] Kotkata M F, Masoud A E, Mohamed M B and Mahmoud E A 2009 *Phys. E Low Dimens. Syst. Nanostruct.* **41** 1457
- [36] Manickathai K, Kasi Viswanathan S and Alagar M 2008 *Indian J. Pure Appl. Phys.* **46** 561
- [37] Chen Y, Xing W, Liu Y, Zhang X, Xie Y, Shen C *et al* 2020 *Nanomaterials (Basel, Switzerland)* **10** 317
- [38] Ali M F B 2020 *RSC Adv.* **10** 44058
- [39] Restrepo G, Valencia S and Marin J M 2010 *Open Mater. Sci. J.* **4** 9
- [40] Murphy A B 2007 *Sol. Energy Mater. Sol. Cells* **91** 1326
- [41] Mexicana De Física S, México A C, Morales E, Mora S, Pal E, Morales A E *et al* 2007 *Rev. Mex. Fis.* **53** 18
- [42] Liu R, Ren F, Su W, He P, Shen C, Zhang L *et al* 2015 *Ceram. Int.* **41** 14615
- [43] Mollavali Majid, Falamaki Cavus and Rohani Sohrab 2015 *Int. J. Hydrog. Energy* **40** 12239
- [44] El Kissani A, Ait Dads H, Oucharrou S, Welatta F, Elaakib H, Nkhaili L *et al* 2018 *Thin Solid Films* **664** 66
- [45] Wu H and Zhang Z 2011 *Int. J. Hydrog. Energy* **36** 13481
- [46] Maneb C B, Khobaree R V, Patild R P and Pawara R P 2018 *Int. J. Appl. Eng. Res.* **13** 14372
- [47] Makuła P, Pacia M and Macyk W 2018 *J. Phys. Chem. Lett.* **9** 6814
- [48] Aguilar Hernández J, Contreras Puente G, Morale Acevedo A, Vigil Galán O, Cruz Gandarilla F, Vidal-Larramendi J *et al* 2003 *Semicond. Sci. Technol.* **18** 111
- [49] Erdogan N, Park J and Ozturk A 2016 *Ceram. Int.* **42** 16766